CARBON 49 (2011) 986–995

available at www.sciencedirect.com

ScienceDirect

journal homepage: www.elsevier.com/locate/carbon

Distribution and biocompatibility studies of graphene oxide in mice after intravenous administration

Xiaoyong Zhang [a,b], *Jilei Yin* [a,c], *Cheng Peng* [a], *Weiqing Hu* [a], *Zhiyong Zhu* [a], *Wenxin Li* [a,*], *Chunhai Fan* [a,*], *Qing Huang* [a,*]

[a] *Laboratory of Physical Biology, Shanghai Institute of Applied Physics, Chinese Academy of Sciences, Shanghai 201800, China*
[b] *Graduate School of Chinese Academy of Sciences, Beijing 100049, China*
[c] *TCM Branch of Jiangsu Uion Technical Institute, Lianyungang 222006, China*

ARTICLE INFO

Article history:
Received 26 May 2010
Accepted 2 November 2010
Available online 10 November 2010

ABSTRACT

We determined the distribution and biocompatibility of graphene oxide (GO) in mice by using radiotracer technique and a series of biological assays. Results showed that GO was predominantly deposited in the lungs, where it was retained for a long time. Compared with other carbon nanomaterials, GO exhibited long blood circulation time (half-time 5.3 ± 1.2 h), and low uptake in reticuloendothelial system. No pathological changes were observed in examined organs when mice were exposed to 1 mg kg^{-1} body weight of GO for 14 days. Moreover, GO showed good biocompatibility with red blood cells. These results suggested that GO might be a promising material for biomedical applications, especially for targeted drug delivery to the lung. However, due to its high accumulation and long time retention, significant pathological changes, including inflammation cell infiltration, pulmonary edema and granuloma formation were found at the dosage of 10 mg kg^{-1} body weight. More attention should be paid to the toxicity of GO.

1. Introduction

Since its isolation in 2004 [1], graphene has attracted tremendous attention due to its unique electronic, thermal, mechanical, and optical properties. Intensive research is ongoing to investigate the quantum physics in this system and potential applications for nanoelectronic devices, transparent conductors, and composite materials [2–9]. Recent studies have showed that GO was useful for biomedical applications, such as drug/gene delivery, biosensing and bioimaging [10–19]. In particular, the potential use of GO as targeted drug delivery vehicle for cancer therapy has attracted considerable interest. Dai and colleagues first demonstrated that GO functionalized with polyethylene glycol was able to delivery aromatic, water-insoluble anticancer drugs into cells, and their intrinsic optical properties were also used for cell imaging [10,11]. Immediately after that, Chen et al. showed that doxorubicin hydrochloride (DXR) could efficiently load onto GO by a simple noncovalent method, the loading ratio of GO could reach 200%, much higher than that of other nanocarriers [12]. They also reported that GO could be modified with magnetic nanoparticle to yield GO based composite, which could move regularly in magnetic field, suggesting that GO may be useful in targeted drug delivery [13]. More recently, Zhang and coworkers reported that GO co-loaded with the two anticancer drugs (doxorubicin (DOX) and camptothecin (CPT)) showed specific targeting to MCF-7 cells, and exhibited remarkably high cytotoxicity when compared to GO loaded with either DOX or CPT only [14]. Moreover, GO was highly physiologically stable and showed excellent biocompatibility

* *Corresponding authors:* Fax: +86 21 59553021.
E-mail addresses: liwenxin@sinap.ac.cn (W. Li), fchh@sinap.ac.cn (C. Fan), huangqing@sinap.ac.cn (Q. Huang).
0008-6223/$ - see front matter
doi:10.1016/j.carbon.2010.11.005

to various cells and bacteria [20–23]. Thus it appears that GO may be a promising candidate like fullerene (C_{60}), carbon nanotubes (CNT), and nanodiamonds (ND) for biomedical applications [10,11,24]. In order to investigate the usefulness of GO in biomedical fields, the experimental information about its adsorption, distribution, metabolism, and excretion (ADME) is urgently needed.

Due to the lack of suitable detection method, little is known about the biological behavior of GO *in vitro*, and no reports have focused on the distribution of GO *in vivo* thus far. Radioactive tracing technique, however, with advantages of high sensitivity, credibility and freedom from interference, has become an excellent approach to obtain information on ADME of nanomaterials *in vivo*. Since ^{99m}Tc labeling of the fullerenol by Li et al. in 2002 [25], numerous studies have been reported on radiolabeling of a variety of carbon nanomaterials (CNM), including C_{60} derivatives [26], single walled carbon nanotubes (SWCNT) [27–29], multi-walled carbon nanotubes (MWNCT) [30,31], and ND [32,33].

The goal of this study was to determine the distribution and pharmacokinetic profiles of GO in mice, and evaluate its biocompatibility with target organs and red blood cells (RBC). Herein, the tissue distribution and clearance of Rhenium (^{188}Re)-GO in mice was determined through an effective and convenient radiotracer technique. Based on the distribution characteristics, its biocompatibility with target organs and RBC was evaluated by a serial of biological assays. The results suggested that ^{188}Re–GO with excellent radiochemical purity and stability is highly suitable for the study of ADME behavior of GO *in vivo*. The relative long blood circulation half time of GO as well as its excellent biocompatibility with target organs and RBC could be beneficial in use of GO for biomedical applications. To the best of our knowledge, this is the first study to address this issue. And we believed this study will contribute significantly to better understanding the toxicity of GO *in vivo* and will encourage the development of GO in biomedical fields in the near future.

2. Materials and methods

2.1. Reagents and animals

^{188}Re was obtained from an alumina-based ^{188}W/^{188}Re generator (Shanghai Ke-Xing Pharmaceutical Co.); loaded with the ^{188}W solution supplied by the Oak Ridge National Laboratory (Oak Ridge, TN). GO was prepared by a modified Hummers method and characterized by atomic force microscopy (AFM) and Raman spectroscopy [34]. All the other chemicals used were of analytical grade, obtained from commercial sources and used without further purification.

Kun Ming mice (Sprague–Dawley rats) were purchased from Shanghai SLAC Laboratory Animal Co., Ltd., China. The animals were housed in plastic cages, fed a commercial diet, and given water ad libitum. All animals were checked for the absence of infection for 1 week prior to experiment. Permission of the local ethics committee was obtained, and all animal experiments were performed according to Chinese law and accepted international standards in biomedical research.

2.2. Labeling of GO with ^{188}Re

The radiolabeling of GO was performed by a conventional reduction method based on our previous report [33]. Briefly, 1 mL of GO (1 mg mL^{-1}), 50 μl ascorbic acid (40 mg mL^{-1}), 70 μl stannous chloride (60 mg mL^{-1}), and 1 mCi Na^{188}ReO$_4$ were reacted in water bath at 80 °C for 25 min. After the end of the reaction, 10 μl portions of the mixture were taken and applied at 1.5 cm from the lower end of the strips for determining the labeling yield by paper chromatograph with Whatman No. 1 (1 cm × 13 cm). The strips were developed by saline solution until the solvent reached the top portions. The strips were dried and cut into 1 cm long equal segments. The distribution of ^{188}Re on paper chromatograph was measured with a gamma-ray counter.

The radioactivity for ^{188}Re–GO are all at the origin on the chromatography paper developed by saline solution (retardation faction, $R_f = 0$), with R_f value for free ReO_4^- ions being at about 0.9–1. And the labeling yield of ^{188}Re–GO was calculated by the following equation:

$$\text{Labeling yield} = Y\,[\text{segment0}]/Y\,[\text{segments(0–10)}] \times 100\%$$

Y [segment 0] represents the counts number of per minute (CPM) of segment 0, while Y [segments (0–10)] represents the CPM of summed over all segments.

2.3. Purification of ^{188} Re–GO and examination of its stability

Before the distribution evaluation, the radiolabeling compound was washed three times with saline to remove unreacted ascorbic acid and stannous chloride. Then the ^{188}Re–GO was dispersed in Millipore water, serum-free culture medium (RPMI-1640 only), and complete culture medium (RPMI-1640 with 10% fetal bovine serum (FBS)) at room temperature, respectively. Portions (10 μl) from each suspension were applied for determining the radiochemical purity by the manner described above. The radiochemical purity of labeled ^{188}Re–GO obtained at various time intervals was used to examine its stability *in vitro*.

To assess the stability of ^{188}Re–GO *in vivo*, 20 Kun Ming mice (male 20 ± 2 g, 6–8 W) were intravenously injected with 200 μl of the ^{188}Re–GO suspension containing 50 μCi of radioactivity. The mice were then anesthetized with pentobarbital sodium at 1, 3, 6, 12, and 24 h post injection, the anticoagulant blood was collected and its radioactivity was measured with gamma-ray counter. Then the blood was centrifuged at 14,000 rpm for 5 min, the supernatant was discarded and the remaining solid was washed with deionized water. Its radioactivity was measured with gamma-ray counter for comparison with the whole blood radioactivity.

2.4. Distribution of GO in mice

The distribution characteristics of GO was performed with 48 Kun Ming mice (male 20 ± 2 g, 6–8 W), which were randomly divided into six groups. Mice were anesthetized with pentobarbital sodium and 20 μCi ^{188}Re–GO was intravenously administrated to each mouse. At different time points, the mice were sacrificed by dislocation of vertebrae, and important organs and tissues were excised, washed, and weighed, radioactive of each tissue was measured with gamma-ray counter. The uptake of the radiolabeled GO in different organs and tissues was expressed as the percentage of the injected dose per gram of tissue (%ID/g), as shown in Eq. (1). The resultant data were expressed as mean values with the standard deviation.

$$\text{Organ uptake} = \frac{\text{Organ radioactivity}}{\text{Total radioactivity} \times \text{organ weight (g)}} \times 100\% \tag{1}$$

2.5. *Histopathological morphology studies*

Based on the distribution results, the organs with high %ID/g values were excised for histopathological analysis. A similar animal experiment procedure as described above was adopted, after a single intravenous injection of 1 and 10 mg kg^{-1} body weight of GO, mice were sacrificed at 14 days post injection. Lungs, liver, spleen, and kidney were collected and fixed with paraformaldehyde for histopathological analysis. All histopathological tests were performed using standard laboratory procedures. The tissues were embedded in paraffin blocks, then sliced into 5 μm thick sections and placed onto glass slides. After hematoxylin–eosin staining, the slides were observed and photographs were taken using an optical microscope (Motorized inverted system microscope IX81/IX81–ZDC, Japan). The pathologist performing the visual analysis was blinded to the sample identifier and results of the other histopathological analyses.

2.6. *Observation of the erythrocyte shape and erythrocyte hemolysis assay*

Fresh blood was obtained from Sprague–Dawley rats and anticoagulated with 3.8% sodium citrate (blood to sodium citrate is 9:1 in volume), then the anticoagulated blood was centrifuged (4000 rpm, 5 min) at 4 °C using a centrifuge himac-CF 16RX (Hitachi, Japan). The plasma and buffy coat were removed by aspiration. The separated erythrocytes were washed three times by centrifugation (4000 rpm, 5 min) in 10 volumes of 10 mM phosphate buffer saline (PBS), which consisted of 125 mM NaCl and 10 mM NaH_2PO_4 and Na_2HPO_4 in deionized water, adjusted to pH 7.4. The supernatant and buffy coat of white cells was carefully removed with each wash. During the last washing, the erythrocytes were obtained by centrifugation (4000 rpm, 5 min). Washed erythrocytes were finally re-suspended to the desired hematocrit level using the same buffer and stored at 4 °C and used within 6 h of sample preparation.

The effect of GO on the erythrocyte shape changes was investigated by optical microscopy. Erythrocyte suspension (10% hematocrit) was incubated with various doses of GO suspension. At different time points, 100 μl of these reaction mixtures were dropped onto glass slide and observed by optical microscopy directly. The observation of the erythrocyte shape changes was carried out at 37 °C using an optical microscope (Motorized inverted system microscope IX81/IX81–ZDC, Japan); the overall magnification was 400×.

The *in vitro* effect of human erythrocyte hemolysis by GO was evaluated according to the procedures described by Ng et al. [35]. An erythrocyte suspension (10% hematocrit) was incubated with GO at different concentrations (in PBS, pH 7.4) up to 6 h. The reaction mixtures were shaken gently while being incubated at 37 °C for 6 h. At intervals of every 60 min, a volume of 200 μL of the reaction mixtures was removed and diluted with 3.8 mL of PBS and centrifuged at 4000 rpm for 10 min. The absorbance of the resulting supernatant (A) was measured at 541 nm by a spectrophotometer U-3010 (Hitachi, Japan). Likewise, the same volume of the reaction mixtures was treated with 3.8 mL of distilled water to obtain a complete hemolysis. The absorbance of its supernatant (B) was measured at the same condition. The percentage hemolysis was calculated from the ratio of the readings $(A/B) \times 100$, which reflected the influence of GO on erythrocyte hemolysis.

3. Results and discussion

3.1. *Preparation and characterization of GO*

GO was prepared by using a modified Hummers method [34]. Analysis of products by AFM revealed mostly single layered GO (>70%) with ~1.0 nm in topographic height and 10–800 nm in lateral width (Fig. 1). No significant amounts of particles were observed on the mica substrate, showing good purity of the GO in solution. The GO solution was stable in pure water for over a month and did not agglomerate.

Fig. 2 shows the Raman spectroscopy of GO by using 632 nm wavelength excitation. The results clearly showed that D-band signal was significantly appeared after graphite treated with concentration sulfuric acid and $KMnO_4$, suggesting that the disorder was introduced onto the graphene layer. The Raman characteristic of GO is consistent with many previous reports [36,37].

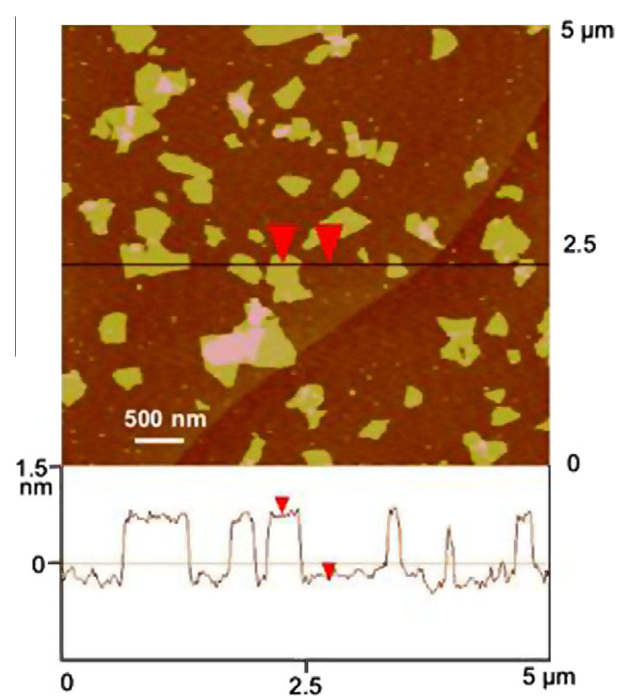

Fig. 1 – Afm image of GO.

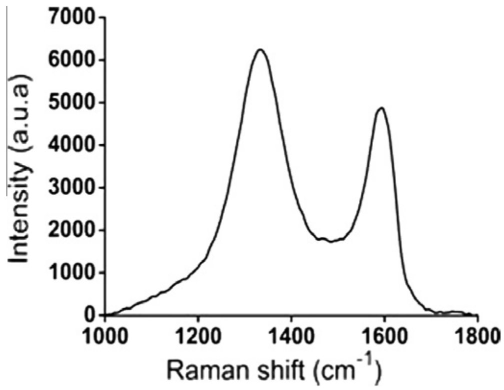

Fig. 2 – Raman spectrum of GO.

3.2. *Labeling, purification and stability studies of ^{188}Re–GO compounds*

The labeling procedure is based on the reduction of Re(VII) to Re(V), which possesses unfilled electron orbits and has strong coordination ability to other molecules. When Re(VII) was reduced into Re(V), the unfilled electron orbits of Re(V) were filled by electrons donated by carboxyl group and hydroxyl group from GO and thus formed a stable labeling complex. The labeling yield of ^{188}Re–GO is over 92% under the labeling conditions described above. Also, in an independent experiment, the water stability of GO and the labeling compounds were characterized by a Nano Zeta Potential and Submicron Particle Size Analyzer (Beckman Coulter Delsa). Results

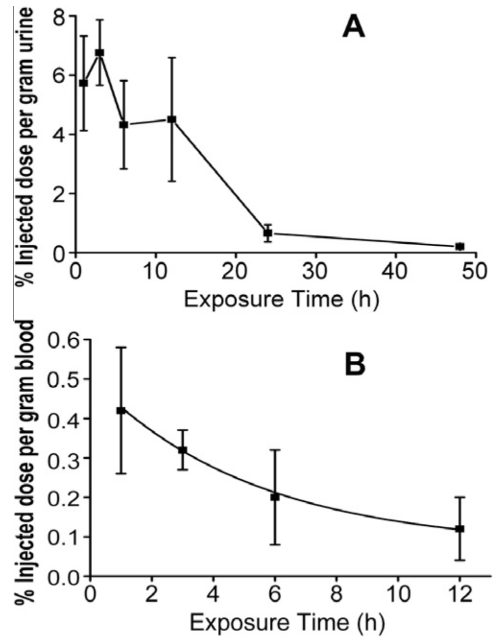

Fig. 3 – Clearance of GO in urine and blood of mice at different time points post injection, (A) clearance curve of urine, (B) clearance curve of blood. Data are presented as mean ± standard standard deviation (n = 8).

Table 1 – Biodistribution of ^{188}Re–GO in Kun Ming mice after intravenous injection at different time points up to 48 h, and each value represents the (%ID/g, mean ± standard deviation) for n = 8 mice for each time points.

Organ	Time after injection					
	1 h	3 h	6 h	12 h	24 h	48 h
Heart	0.36 ± 0.09	0.27 ± 0.04	0.25 ± 0.08	0.16 ± 0.05	0.27 ± 0.11	0.32 ± 0.16
Liver	2.83 ± 0.47	5.9 ± 2.01	4.66 ± 0.74	4.21 ± 0.64	3.04 ± 0.37	2.88 ± 0.49
Spleen	2.85 ± 1.60	4.52 ± 1.80	3.62 ± 0.59	2.96 ± 0.59	4.11 ± 1.63	2.41 ± 0.93
Lung	40.34 ± 10.14	36.06 ± 10.18	31.99 ± 2.64	30.44 ± 3.87	32.76 ± 12.24	25.53 ± 6.27
Kidney	0.69 ± 0.09	0.7 ± 0.08	0.56 ± 0.22	0.34 ± 0.11	0.18 ± 0.02	0.19 ± 0.04
Brain	0.04 ± 0.01	0.04 ± 0.00	0.04 ± 0.01	0.03 ± 0.01	0.03 ± 0.01	0.03 ± 0.01
Bone	0.26 ± 0.14	0.38 ± 0.08	0.34 ± 0.14	0.51 ± 0.37	0.74 ± 0.28	0.12 ± 0.04
Stomach	1.25 ± 0.34	1.43 ± 0.35	0.81 ± 0.41	0.45 ± 0.31	0.14 ± 0.05	0.06 ± 0.01

Table 2 – Distribution characteristics of GO compared with other CNM *in vivo* after 24 h intravenous injection.

CNM	Ratio of %ID/g values in organs			Blood circulation half-time (h)	References
	Lungs/liver[a]	Lungs/spleen[b]	Lungs/kidney[c]		
GO	>10	>8	>150	5.3	This study
SWCNT	<0.5	<1	<1	1	[28,29,39,41,42]
MWCNT	<0.5	<3	<1	–	[31,43]
C_{60}	<0.5	<0.5	<2	<3	[25,44]
ND	<0.2	<5	<5	–	[32]

[a] Lungs/liver represents the ratio between %ID/g values of lungs and liver.
[b] Lungs/spleen represents the ratio between %ID/g values of lungs and spleen.
[c] Lungs/kidney represents the ratio between %ID/g values of lungs and spleen.

showed that the values of zeta potential of GO and Re–GO in water are −29.87 and −20.47, respectively, suggesting that the reduction reaction has only a small impact on the physicochemical properties of GO.

Prior to the experiments of distribution of ^{188}Re–GO, the labeled compounds were needed to carry out further purification to remove the unreacted stannous chloride, ascorbic acid, and free $NaReO_4$. By simple triple purification cycles of centrifugation and washing with saline, as indicated by analysis of the paper chromatography, the typical radiochemical purity of the ^{188}Re–GO increased from 92.2% to 98.5% (data not shown).

In vitro stability of ^{188}Re–GO was examined by checking their radiochemical purities at various elapsed times with the paper chromatography technique. Results showed that ^{188}Re–GO is very stable in three kinds of media tested in this work (pure water, RPMI-1640 (FBS free), and complete cell culture medium (RPMI-1640 with 10% FBS), with the radiochemical purity of the labeling compounds kept greater than 90% even after 48 h (data not shown). In addition, ^{188}Re–GO showed excellent stability in mice. About 67% ^{188}Re–GO kept intact in blood even at 24 h post injection, suggesting that the distribution resulted from the counting of the ^{188}Re–GO radioactivity in this work was the real distribution of GO in mice, rather than that of radionuclide ^{188}Re, which may fall from the ^{188}Re–GO.

3.3. *Distribution of ^{188}Re–GO in mice*

The distribution data of ^{188}Re–GO in mice were obtained from the radioactive measurement. As shown in Table 1, the GO (^{188}Re–GO) was apparently cleared from the blood stream rapidly and distributed throughout most of the organs within 48 h, but the accumulation was primarily in the lungs, liver, and spleen, with to much less extent in the brain, heart, and bone. As time elapsed, gradual decrease was observed in most organs, except for liver, and spleen. However, it is worth noting that the GO was retained in lungs, liver, and spleen at the relatively high accumulation levels for a long time. At 48 h post injection, there was considerable amounts of GO in lungs (25.53 ± 6.27%ID/g), liver (2.88 ± 0.49%ID/g), and spleen (2.41 ± 0.93%ID/g). The high-level accumulation of GO in organs such as lungs, liver, and spleen suggested that the rapid uptake of the GO was intercepted by the mononuclear phagocytes in the reticuloendothelial system (RES). Such an uptake mechanism involving RES is consistent with the general conception on the fate of nanoparticles *in vivo*.

The high-level accumulation of GO in lungs also allowed direct observation of digested tissue solutions. In an independent experiment, mice were exposed to 400 μg of GO and sacrificed at 30 min, 1 and 3 days post injection, respectively. Tissues (about 0.5 g liver, and the whole lung and spleen) were collected and then digested with 2 mL of a mixture of 65%

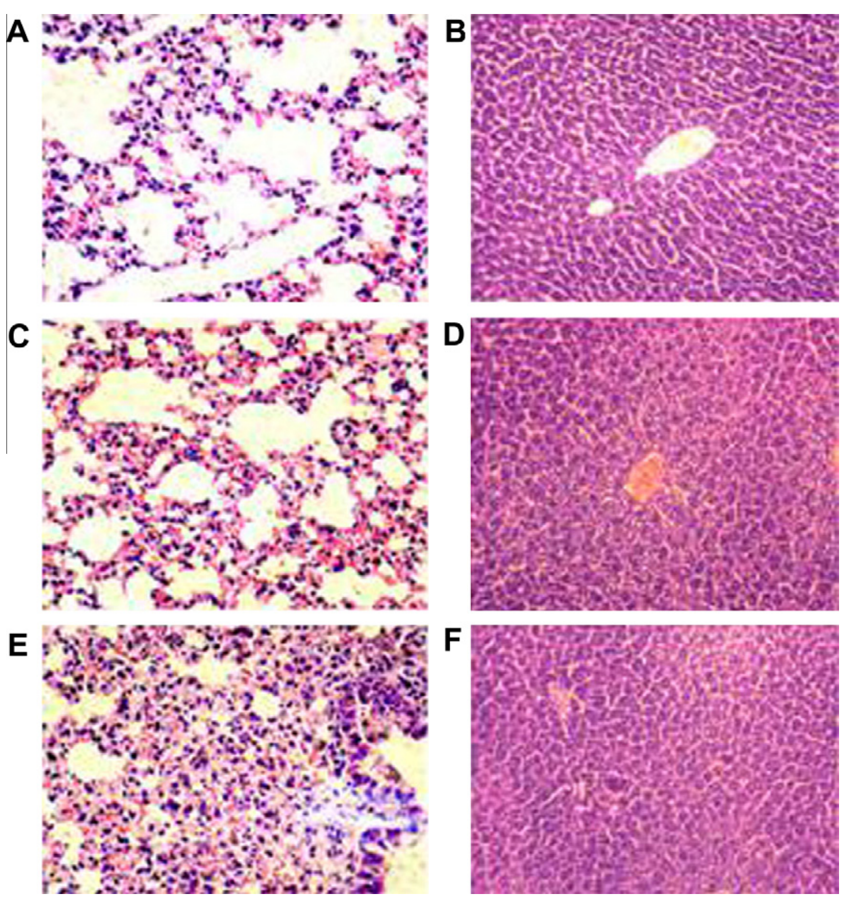

Fig. 4 – Histopathology of the lung (left) and liver (right) tissue (100×) in male mice 14 days post injection to GO by a single intravenous injection of control group (only exposed to 0.2 mL PBS) (A and B), 1 mg kg^{-1} body weight group (C and D), 10 mg kg^{-1} body weight group (E and F).

$HClO_4$ and 30% H_2O_2 (1:1 in volume) at 90 °C for 1 h. After centrifugation (10,000 rpm × 10 min), the digested solution was blackcolored, much more dark color was found in lung digestion solution than liver and spleen (not shown), indicated that much high accumulation of GO in lungs than that of in liver or spleen.

In addition, to examine the clearance of GO from mice, the radioactivity intensity in urine was measured at different time points up to 48 h. Fig. 3A shows a plot of values of %ID/g in urine vs. time points post injection. As illustrated by the clearance curve, we observed the relative high values of %ID/g in urine within 12 h; however, the radioactivity in the urine was much lower and almost no detectable at 24 and 48 h post injection (Fig. 3A). The distinctive clearance behavior of GO was likely ascribed to the inhomogeneous nature of GO. Fig. 1 clearly showed that the lateral width of GO is various from several nanometers to several hundred nanometers, the various distribution of lateral width of GO may lead to some GO particles with small size were quickly eliminated through renal route, which exhibited relative high radioactivity in urine within 12 h post injection. However, most of GO particles with large size were intercepted by lungs, thus leading to high accumulation level of GO in lungs. The high uptake of GO in lungs was hard to excrete (Table 1), which is consistent with the radioactivity intensity in urine at 24 and 48 h post injection (Fig. 3A).

The distribution and clearance characteristics of GO, including slow excretion through renal excretion route and long time accumulation in organs are significant different from the pervious reports by Singh et al. [28,38]. They demonstrated that f-SWCNT/f-MCWNT labeled with ^{111}In was not retained in any of the organs such as liver or spleen and rapidly cleared from systemic circulation through the renal excretion route. But the high-level accumulation of GO in target organs is similar to many other reports. For example, Sun et al. using isotope ratio mass spectroscopy to determine the ^{13}C-enriched SWCNT and found that SWCNT were distributed in the entire body, with major accumulation in liver, lungs, and spleen over 3 months [39–41].

Furthermore, we also investigated the blood circulation half time of GO in mice. Fig. 3B showed that, as time elapsed, the radioactivity in blood was gradually decreased within 24 h. And as illustrated by the solid curve, the data are well modeled by first-order (exponential) decay with a half-life of 5.3 ± 1.2 h, which is much longer than the SWCNT (1.0 ± 0.1 h) and fullerene (C_{60}) [25,40]. The relative long blood circulation half time suggested that GO may be a promising candidate for biomedical applications, especially for targeted drug delivery.

In conclusion, compared with other CNM, such as SWCNT, MWCNT, C_{60}, and ND, GO showed extremely high accumulation in lungs, with relative long blood circulation time and low uptake by RES. As illustrated by Table 1, the %ID/g values

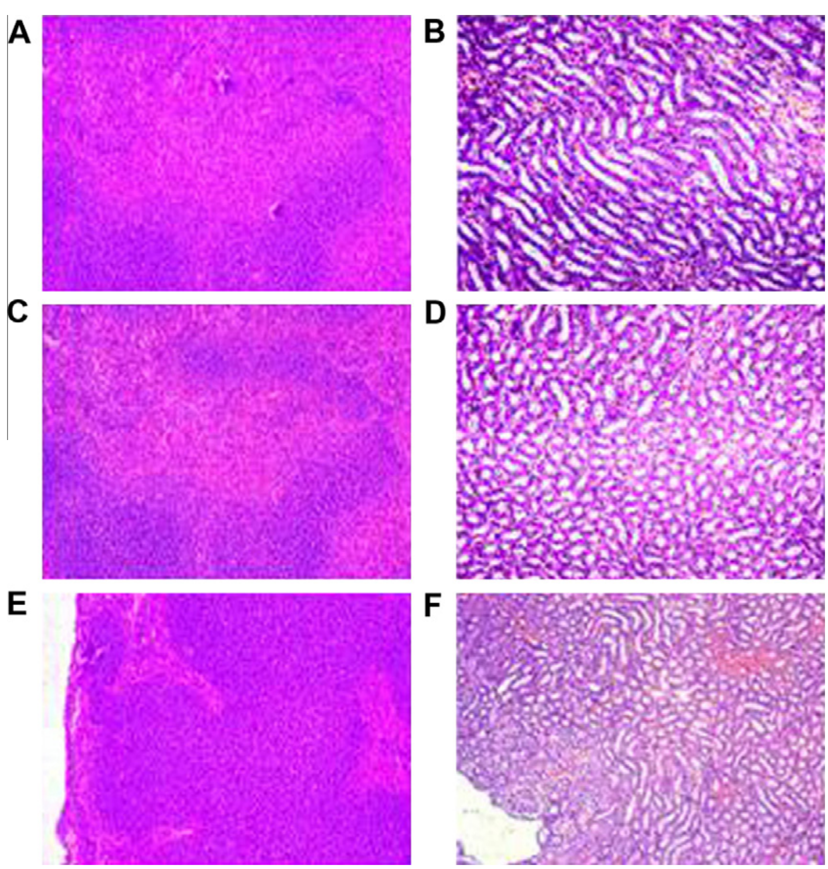

Fig. 5 – Histopathology of the spleen (left) and kidney (right) tissue (100×) in male mice 14 days post injection to GO by a single intravenous injection of control group (only exposed to 0.2 ml PBS) (A and B), 1 mg kg^{-1} body weight group (C and D), 10 mg/kg mg kg^{-1} body weight group (E and F).

for lungs, liver, and spleen were 32.76 ± 12.24%, 3.04 ± 0.37%, and 4.11 ± 1.63% at 24 h post injection, respectively. Considered the ratio between the %ID/g values of lungs and other organs, the ratio values of lungs/liver, lungs/spleen, and lungs/kidney are greater than 10, 8, and 150, respectively, which are much higher than the other CNM (Table 2). In addition, it is worth pointing out that GO showed relative longer blood circulation half time (≈5.3 h) than the other CNM [25,40]. The difference distribution and clearance characteristics in the CNM is likely due to the surface chemistry of GO from the other CNM. And the relative long blood circulation half time and low uptake by the RES are largely attributing to its distinctive physicochemical properties, such as small size, high water dispersion, and unique structure characteristics.

3.4. *Histopathological morphology analysis of GO in mice*

Based on the distribution of GO in mice, we checked the pathological changes in the targeted organs, such as lungs, liver, spleen, and kidney with 1 or 10 mg kg^{-1} body weight of GO at 14 days post injection. The representative micrographs from each group at day 14 after GO injection are depicted in Figs. 4 and 5. No pathological changes were observed in the examined organs, such as lungs, liver, spleen, and kidney when mouse treated with 1 mg kg^{-1} body weight of GO for 14 days, and no significant pathological changes were observed in liver, spleen, and kidney even at the dosage of 10 mg kg^{-1} body weight (in Figs. 4 and 5). However, due to the high-level accumulation and slow clearance, we did observed significant pathological changes, including granulomatous lesions, pulmonary edema, inflammatory cell infiltration, and fibrosis throughout the lung for the group treated with 10 mg kg^{-1} body weight of GO (Fig. 4E). These results suggested that GO is biocompatible in most tissues but caution about lung pathologies at higher doses. Although previous studies demonstrated that GO were biocompatibility with various cell lines, thus far no studies have reported its toxicity *in vivo*. As the first report focused on the *in vivo* toxicity of GO, it is an important step for the practical biomedical applications of GO in the near future.

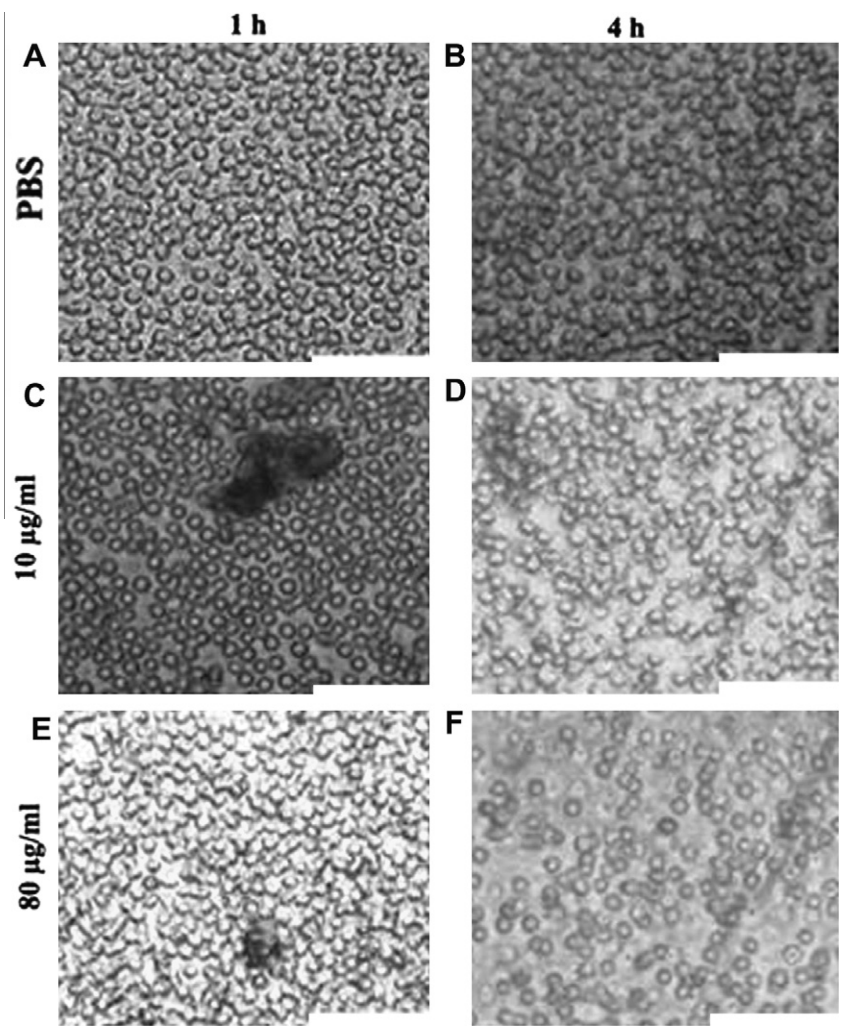

Fig. 6 – Effect of concentration of GO and incubation time on the morphological changes of human erythrocytes. (A) Exposures to PBS for 1 h. (B) Exposures to PBS for 4 h. (C) Exposures to GO suspension 10 µg mL^{-1} for 1 h. (D) Exposures to GO suspension 10 µg $mL^{-1}$for 4 h. (E) Exposures to GO suspension 80 µg mL^{-1} for 1 h. (F) exposures to GO suspension 80 µg mL^{-1} for 4 h. Scale bar = 50 µm.

3.5. *Observation of the erythrocyte shape and erythrocyte hemolysis*

Optical microscopy analysis of erythrocyte morphology after incubated with PBS, 10 and 80 $\mu g\,mL^{-1}$ GO suspension was shown in Fig. 6. We found that almost all the erythrocyte membranes were kept integrated when they incubated with PBS for up to 4 h (Fig. 6A and B). Although GO flakes were adhered to the surface of RBC, GO suspension showed little effect on the erythrocyte morphology and membrane integrity at the dosage of 10 $\mu g\,mL^{-1}$ for 1 and 4 h (Fig. 6C and D). However, a part of erythrocyte membranes were ruptured and ghost cells were observed when erythrocytes exposed to 80 $\mu g\,mL^{-1}$ of GO for 4 h (Fig. 6F).

The good biocompatibility of GO to RBC was further evidenced by hemolysis assay. As shown in Fig. 7A, we found that the hemoglobin has two absorbance peaks at 541 and 576 nm, and there is a well linear relationship between hemoglobin concentration and the absorbance value of 541 nm (not shown). In the present experiment, the effect of GO on the hemolysis was determined based on the absorbance of 541 nm. It can be seen that GO could induce dose and time dependent hemolysis. It can be seen that no significant difference was found between RBC exposure to PBS and GO suspension at the dosage of 10–80 $\mu g\,mL^{-1}$ at 1 h. However, there is about 6.4% hemolysis was induced by incubated with PBS for 6 h and 18.5% hemolysis was induced by 80 $\mu g\,mL^{-1}$ GO suspension (Fig. 7B). Compared to the previous report by McFetridge [45], GO showed better biocompatibility with RBC than SWCNT, they found that about 11% RBC were hemolysis by unrefined SWCNT within 15 min. The biocompatibility of GO with blood cells is consistent with previous studies, which suggested that GO are biocompatibility with various cells and bacteria [20–23]. In this work, we first evidenced that GO is biocompatibility with blood cells, which will pave the way for further development of GO for targeted drug delivery and other biomedical applications.

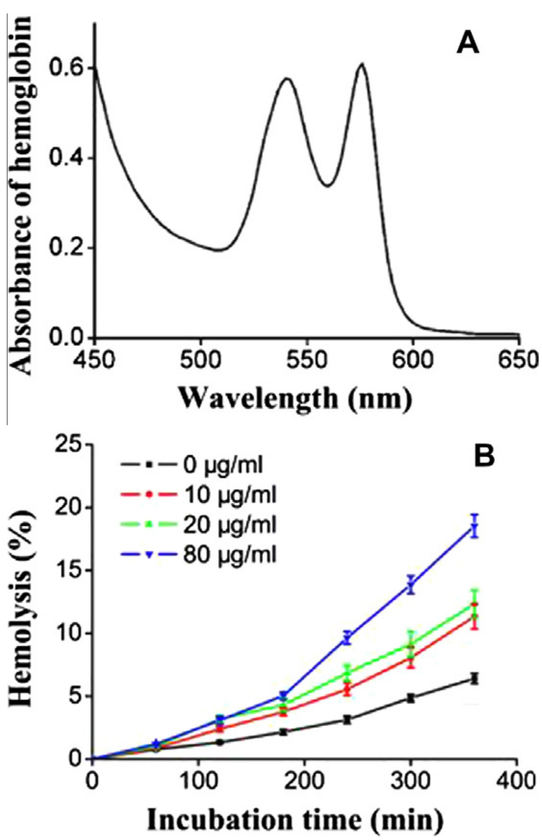

Fig. 7 – (A) UV–Vis absorbance spectroscopy of hemoglobin between 450 and 650 nm (absorption peak at 514 and 576 nm). (B) Hemolysis curve of erythrocytes submitted to GO suspension. Erythrocyte suspension (10% hematocrit) in 10 mM PBS (pH 7.4) was incubated with GO suspension at different concentrations (finally GO concentration at 0, 10, 20, and 80 $\mu g\,mL^{-1}$) for up to 6 h in a shaking water-bath under air atmosphere at 37 °C. Black line, 0 $\mu g\,mL^{-1}$; red line, 10 $\mu g\,mL^{-1}$; green line, 20 $\mu g\,mL^{-1}$; blue line, 80 $\mu g\,mL^{-1}$. The results are expressed as the mean of five experiments.

4. Conclusions

We presented the distribution and biocompatibility profiles of GO in Kun Ming mice. High uptake and long term retention of GO in lungs were demonstrated by using radiotracer technique. And compared with other CNM, GO exhibited relative long blood circulation time (half-time 5.3 ± 1.2 h), and low uptake by RES. The difference distribution characteristics in CNM is likely due to the surface chemistry of GO from other CNM. No significant pathological changes were observed in all the examined organs when mice were exposed to 1 $mg\,kg^{-1}$ of GO for 14 days. And compared with SWCNT, GO exhibited less adverse effects on RBC. These results suggested the potential biomedical applications of GO, especially for targeted drug delivery to the lung. However, it is worth noting that the high uptake of GO in lungs was hard to excrete, thus may lead to adverse effect on these organs. In this work, we observed significant pathological changes including inflammation cell infiltration, pulmonary edema, and granuloma formation in the lung of mice when mice were exposed to 10 $mg\,kg^{-1}$ body weight of GO for 14 days. This reminded us much more attention should be paid to the toxicity of highly dosed GO, including acute and chronic toxicity to the lung and other target organs. In the present work, however, we only provided the preliminary information on toxicity of GO in mice; further experimental verification and mechanistic elucidation are required before GO widely used for biomedical applications.

Acknowledgements

This work was supported by the National Science Foundation of China (Nos. 10775169, 10905086, 10975179), the Shanghai Municipal Natural Science Foundation (Nos. 08ZR1422700, 08JC1422600), the ministry of Health (No. 2009ZX10004-301), the CAS Innovation Program (No. 095501K), and the MOST973 Program (No. 2006CB705605).

REFERENCES

[1] Novoselov KS, Geim AK, Morozov SV, Jiang D, Zhang Y, Dubonos SV, et al. Electric field effect in atomically thin carbon films. Science 2004;306(5696):666–9.

[2] Geim AK, Novoselov KS. The rise of graphene. Nat Mater 2007;6(3):183–91.

[3] Stankovich S, Dikin DA, Dommett GHB, Kohlhaas KM, Zimney EJ, Stach EA, et al. Graphene-based composite materials. Nature 2006;442(7100):282–6.

[4] Liu Y, Zhou J, Zhang X, Liu Z, Wan X, Tian J, et al. Synthesis, characterization and optical limiting property of covalently oligothiophene-functionalized graphene material. Carbon 2009;47(13):3113–21.

[5] Liang J, Huang Y, Zhang L, Wang Y, Ma Y, Guo T, et al. Molecular-level dispersion of graphene into poly (vinyl alcohol) and effective reinforcement of their composites. Adv Funct Mater 2009;19(14):2297–302.

[6] Zhou X, Huang X, Qi X, Wu S, Xue C, Boey FYC, et al. In situ synthesis of metal nanoparticles on single-layer graphene oxide and reduced graphene oxide surfaces. J Phys Chem C 2009;113(25):10842–6.

[7] Li B, Lu G, Zhou X, Cao X, Boey F, Zhang H. Controlled assembly of gold nanoparticles and graphene oxide sheets on dip pen nanolithography-generated templates. Langmuir 2009;25(18):10455–8.

[8] Yin Z, Wu S, Zhou X, Huang X, Zhang Q, Boey F, et al. Electrochemical deposition of ZnO nanorods on transparent reduced graphene oxide electrodes for hybrid solar cells. Small 2009;6(2):307–12.

[9] Qi X, Pu KY, Zhou X, Li H, Liu B, Boey F, et al. Conjugated-polyelectrolyte-functionalized reduced graphene oxide with excellent solubility and stability in polar solvents. Small 2010;6(5):663–9.

[10] Liu Z, Robinson JT, Sun X, Dai H. PEGylated nano-graphene oxide for delivery of water insoluble cancer drugs. J Am Chem Soc 2008;130(33):10876–7.

[11] Sun X, Liu Z, Welsher K, Robinson JT, Goodwin A, Zaric S, et al. Nano-graphene oxide for cellular imaging and drug delivery. Nano Res 2008;1(3):203–12.

[12] Yang X, Zhang X, Liu Z, Ma Y, Huang Y, Chen Y. High-efficiency loading and controlled release of doxorubicin hydrochloride on graphene oxide. J Phys Chem C 2008;112(45):17554–8.

[13] Yang X, Zhang X, Ma Y, Huang Y, Wang Y, Chen Y. Superparamagnetic graphene oxide–Fe_3O_4 nanoparticles hybrid for controlled targeted drug carriers. J Mater Chem 2009;19(18):2710–4.

[14] Zhang L, Xia J, Zhao Q, Liu L, Zhang Z. Functional graphene oxide as a nanocarrier for controlled loading and targeted delivery of mixed anticancer drugs. Small 2009;6(4):537–44.

[15] Lu CH, Yang HH, Zhu CL, Chen X, Chen GN. A graphene platform for sensing biomolecules. Angew Chem Int Ed 2009;48(26):4785–7.

[16] He S, Song B, Di Li CZ, Qi W, Wen Y, Wang L, et al. A graphene nanoprobe for rapid, sensitive, and multicolor fluorescent DNA analysis. Adv Funct Mater 2010;20(3):453–9.

[17] Wang Y, Lu J, Tang L, Chang H, Li J. Graphene oxide amplified electrogenerated chemiluminescence of quantum dots and its selective sensing for glutathione from thiol-containing compounds. Anal Chem 2009;81(23):9710–5.

[18] Wang Z, Zhou X, Zhang J, Boey F, Zhang H. Direct electrochemical reduction of single-layer graphene oxide and subsequent functionalization with glucose oxidase. J Phys Chem C 2009;113(32):14071–5.

[19] Lu CH, Zhu CL, Li J, Liu JJ, Chen X, Yang HH. Using graphene to protect DNA from cleavage during cellular delivery. Chem Commun 2010;46:3116–8.

[20] Agarwal S, Zhou X, Ye F, He Q, Chen GCK, Soo J, et al. Interfacing live cells with nanocarbon substrates. Langmuir 2010;26(4):2244–7.

[21] Akhavan O, Ghaderi E. Photocatalytic reduction of graphene oxide nanosheets on TiO_2 thin film for photoinactivation of bacteria in solar light irradiation. J Phys Chem C 2009;113(47):20214–20.

[22] Park S, Mohanty N, Suk JW, Nagaraja A, An J, Piner RD, et al. Biocompatible, robust free-standing paper composed of a TWEEN/graphene composite. Adv Mater 2010;22(15):1736–40.

[23] Liu Y, Yu D, Zeng C, Miao Z, Dai L. Biocompatible graphene oxide-based glucose biosensors. Langmuir 2010;26(9):6158–60.

[24] Bianco A, Kostarelos K, Prato M. Applications of carbon nanotubes in drug delivery. Curr Opin Chem Biol 2005;9(6):674–9.

[25] Li Q, Xiu Y, Zhang X, Liu R, Du Q, Shun X, et al. Preparation of $^{99m}Tc\text{-}C_{60}(OH)_x$ and its biodistribution studies. Nucl Med Biol 2002;29(6):707–10.

[26] Xu JY, Li QN, Li JG, Ran TC, Wu SW, Song WM, et al. Biodistribution of $^{99m}Tc\text{-}C_{60}(OH)_x$ in Sprague-Dawley rats after intratracheal instillation. Carbon 2007;45(9):1865–70.

[27] Wang H, Wang J, Deng X, Sun H, Shi Z, Gu Z, et al. Biodistribution of carbon single-wall carbon nanotubes in mice. J Nanosci Nanotechnol 2004;4(8):1019–24.

[28] Singh R, Pantarotto D, Lacerda L, Pastorin G, Klumpp C, Prato M, et al. Tissue biodistribution and blood clearance rates of intravenously administered carbon nanotube radiotracers. Proc Natl Acad Sci USA 2006;103(9):3357–62.

[29] Liu Z, Cai W, He L, Nakayama N, Chen K, Sun X, et al. *In vivo* biodistribution and highly efficient tumour targeting of carbon nanotubes in mice. Nat Nanotechnol 2006;2(1):47–52.

[30] Guo J, Zhang X, Li Q, Li W. Biodistribution of functionalized multiwall carbon nanotubes in mice. Nucl Med Biol 2007;34(5):579–83.

[31] Deng X, Yang S, Nie H, Wang H, Liu Y. A generally adoptable radiotracing method for tracking carbon nanotubes in animals. Nanotechnology 2008;19:075101.

[32] Yuan Y, Chen Y, Liu JH, Wang H, Liu Y. Biodistribution and fate of nanodiamonds *in vivo*. Diam Relat Mater 2009;18(1):95–100.

[33] Zhang X, Yin J, Kang C, Li J, Zhu Y, Li W, et al. Biodistribution and toxicity of nanodiamonds in mice after intratracheal instillation. Toxicol Lett 2010;198(2):237–43.

[34] Hummers Jr WS, Offeman RE. Preparation of graphitic oxide. J Am Chem Soc 1958;80(6):1339.

[35] Ng TB, Liu F, Wang ZT. Antioxidative activity of natural products from plants. Life Sci 2000;66(8):709–23.

[36] Yang D, Velamakanni A, Bozoklu G, Park S, Stoller M, Piner RD, et al. Chemical analysis of graphene oxide films after heat and chemical treatments by X-ray photoelectron and micro-Raman spectroscopy. Carbon 2009;47(1):145–52.

[37] Compagnini G, Giannazzo F, Sonde S, Raineri V, Rimini E. Ion irradiation and defect formation in single layer graphene. Carbon 2009;47(14):3201–7.

[38] Lacerda L, Soundararajan A, Singh R, Pastorin G, Al-Jamal KT, Turton J, et al. Dynamic imaging of functionalized multi-walled carbon nanotube systemic circulation and urinary excretion. Adv Mater 2007;20(2):225–30.

[39] Cherukuri P, Gannon CJ, Leeuw TK, Schmidt HK, Smalley RE, Curley SA, et al. Mammalian pharmacokinetics of carbon nanotubes using intrinsic near-infrared fluorescence. Proc Natl Acad Sci USA 2006;103(50):18882–6.

[40] Yang S, Guo W, Lin Y, Deng X, Wang H, Sun H, et al. Biodistribution of pristine single-walled carbon nanotubes *in vivo*. J Phys Chem C 2007;111(48):17761–4.
[41] Liu Z, Davis C, Cai W, He L, Chen X, Dai H. Circulation and long-term fate of functionalized, biocompatible single-walled carbon nanotubes in mice probed by Raman spectroscopy. Proc Natl Acad Sci USA 2008;105(5):1410–5.
[42] Yang ST, Fernando KAS, Liu JH, Wang J, Sun HF, Liu Y, et al. Covalently PEGylated carbon nanotubes with stealth character *in vivo*. Small 2008;4(7):940–4.
[43] Deng X, Jia G, Wang H, Sun H, Wang X, Yang S, et al. Translocation and fate of multi-walled carbon nanotubes *in vivo*. Carbon 2007;45(7):1419–24.
[44] Ji ZQ, Sun H, Wang H, Xie Q, Liu Y, Wang Z. Biodistribution and tumor uptake of $C_{60}(OH)_x$ in mice. J Nanopart Res 2006;8(1):53–63.
[45] Crouzier T, Nimmagadda A, Nollert MU, McFetridge PS. Modification of single walled carbon nanotube surface chemistry to improve aqueous solubility and enhance cellular interactions. Langmuir 2008;24(22):13173–81.